ARTICLE

Synthesis and Reactivity of a Benzo-Fused 1,2-Diborete Biradicaloid

Received 00th January 20xx,
Accepted 00th January 20xx

DOI: 10.1039/x0xx00000x

Alena Häfner,[a,b] Lukas Endres,[a,b] Merle Arrowsmith,[a,b] Cornelius Mimh,[a,b] Sonja Fuchs,[a,b] Samuel Nees,[a,b] Krzystof Radacki,[a,b] Ivo Krummenacher,[a,b] Rüdiger Bertermann,[a,b] Felipe Fantuzzi,[c] Holger Braunschweig[a,b,*]

The synthesis of 1,2-$(BCl_2)_2C_6H_4$ (**1**) was optimised by performing a $SiMe_3$-BCl_2 metathesis reaction between 1-$SiMe_3$-2-$(BCl_2)C_6H_4$ with BCl_3 in the dilute gas phase at 95 °C, with 5-9% of its *meta*-isomer 1,3-$(BCl_2)_2C_6H_4$ (**2**) formed as an inseparable byproduct. The addition of two equiv. of I*i*Pr (1,3-di*iso*propylimidazol-2-ylidene) or CAAC (1-(2,6-di*iso*propylphenyl)-3,3,5,5-tetramethylpyrrolidin-2-ylidene) to **1** yielded the twofold carbene adducts **3-I*i*Pr** and **3-CAAC**, alongside their minor 1,3-isomers **4-I*i*Pr** and **4-CAAC**. In CH_2Cl_2 **3-CAAC** converted into the chloride-bridged boronium cation **5**, with an unusual linear HCl_2^- counteranion. The twofold reduction of **3-I*i*Pr** yielded the doubly fused $C_9B_2N_2$ heterocycle **6**, presumably via an unstable 4π-antiaromatic 1,2-diborete intermediate (**7**) undergoing intramolecular ring expansion of one I*i*Pr ligand and B=B bond splitting. In contrast, **3-CAAC** (or **5**) underwent stepwise reduction to the monoboryl radical **8** ($1e^-$), the bis(boryl) biradical **9** ($2e^-$), the benzo-fused 1,2-diborete biradical **10** ($4e^-$), and the closed-shell diborete dianions **11-M** ($6e^-$, M = Li, Na, K). Furthermore, the reduction of **5** under CO atmosphere yielded a mixture of the benzo-bridged diborylketone **12** and the bis((CAAC,CO)borylene) **12**, the latter being accessible selectively by adduct formation of diborete **10** with CO. EPR spectroscopy and computational analyses confirmed the biradical nature of **10**, with an open-shell singlet ground state and a thermally accessible triplet state, while nucleus-independent chemical shift (NICS) calculations indicate a small but non-negligible 2π-aromatic character for **10**.

Introduction

In recent years, boron-doped heterocycles and materials have attracted significant interest due to their unique electronic properties, which differ markedly from those of their all-carbon analogues.[1-4] With boron being slightly larger than carbon as well as intrinsically electron-deficient, its incorporation into conjugated carbocycles results in a loss of symmetry, a narrower HOMO-LUMO gap, and heightened reactivity. Smaller three-, four- and five-membered boracycles, for example, are far more prone than their carbon counterparts to strain-alleviating ring-expansion reactions by substrate insertion into their relatively labile endocyclic B–C bond(s), thus providing a versatile platform for accessing larger, variously heteroatom-doped boracycles.[5-11] Moreover, some diboron-doped heterocycles are capable of activating small molecules like H_2, CO or CO_2 in a manner reminiscent of transition metal chemistry.[12-18]

In 1983, van der Kerk and coworkers were the first to report the synthesis of a dihydrodiborete, i.e., a 2π-aromatic diboracycle isoelectronic with the cyclobutene dication (Scheme 1a), by reduction of di-*tert*-butylacetylene in the presence of $MeBBr_2$, which likely proceeds via a 1,2-diborylethylene intermediate (Scheme 1b).[19] Based on mass spectrometry and computational evidence, they concluded that the puckered 1,3-isomer **II^{tBu}-Me** was formed, rather than the 1,2-isomer **I^{tBu}-Me**. This was confirmed a year later by the group of Siebert, who isolated and structurally characterised the amino-substituted 1,3-dihydro-1,3-diborete **II^{tBu}-NMe$_2$**, via a similar route.[20] Computations showed that, while the 1,2-isomer **I** is the kinetic product of the reduction, it undergoes facile rearrangement to the thermodynamically favoured 1,3-isomer **II**,[21-23] which is puckered like the cyclobutene dication, yet remains aromatic.[24-26] Interestingly, Berndt showed that 1,3-dihydro-1,3-diboretes can undergo one-electron reduction to the corresponding 3π-electron radical anions.[27]

Unlike **I^{tBu}-NMe$_2$**, the 1,2-diamino-1,2-dihydro-1,2-diborete **I^{H}-N*i*Pr$_2$** can be isolated at room temperature and converted to its 1,3 isomer by heating (Scheme 1c).[28] The isomerisation can also be prevented by benzannellation of the C=C unit, leading to the isolation of the stable 1,2-dihydro-1,2-benzo[b]diborete **III**.[29] In terms of reactivity, the 1,2-dihydro-1,2-diboretes **I^{H}-N*i*Pr$_2$** and **III** undergo Pd-catalysed and NaK-induced

[a] *Institute for Inorganic Chemistry, Julius-Maximilians-Universität Würzburg, Am Hubland, 97074 Würzburg, Germany. E-mail: h.braunschweig@uni-wuerzburg.de*
[b] *Institute for Sustainable Chemistry & Catalysis with Boron, Julius-Maximilians-Universität Würzburg, Am Hubland, 97074 Würzburg, Germany.*
[c] *Chemistry and Forensic Science, School of Natural Sciences, University of Kent, Park Wood Rd, Canterbury CT2 7NH, United Kingdom.*

Electronic Supplementary Information (ESI) available: Synthetic procedures, NMR, EPR and IR spectra, X-ray crystallographic and computational details. CCDC 2411656-2411665. For ESI and crystallographic data in CIF or other electronic format see: DOI: 10.1039/x0xx00000x

dimerisation, respectively, to the corresponding eight-membered 1,2,5,6-tetrahydro-1,2,5,6-tetraborocines,[29-31] while **III** undergoes twofold Pd-catalysed [2+2] cycloaddition with dimethyl acetylenedicarboxylate to generate the corresponding benzo-fused 1,4-dihydro-1,4-diborocine,[29] and photolytic B–B bond cleavage upon reaction with $Fe(CO)_5$, yielding an Fe(0) tricarbonyl η^4-1,4-dibora-1,3-butadiene complex.[32]

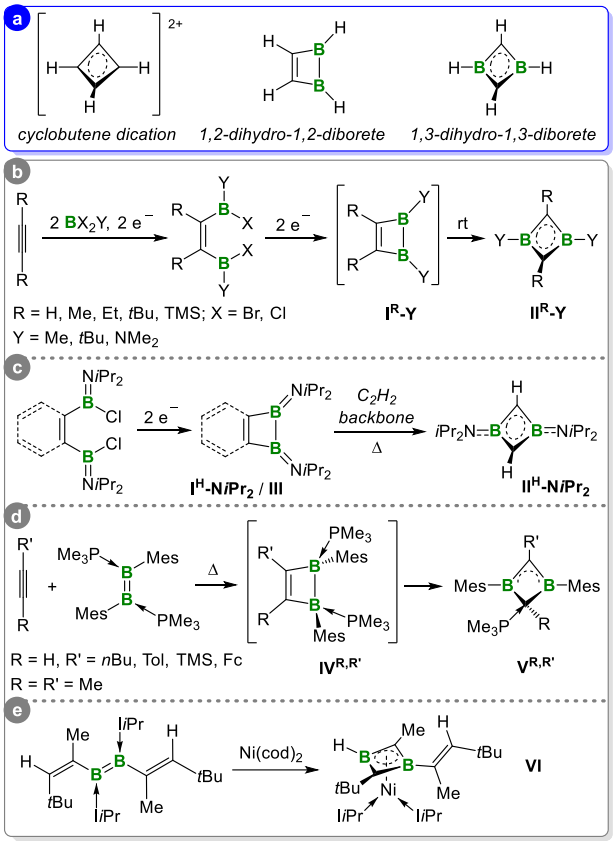

Scheme 1. Synthetic routes to the 1,2- and 1,3-isomers of dihydrodiboretes. TMS = trimethylsilyl, Dur = duryl (2,3,5,6-tetramethylphenyl), Mes = mesityl (2,4,6-trimethylphenyl) Tol = *p*-tolyl, Fc = ferrocenyl.

Our group has also reported the synthesis of phosphine-stabilised 1,3-dihydro-1,3-diboretes (**V$^{R,R'}$**) via [2+2] cycloaddition between doubly PMe_3-stabilised 1,2-diaryldiborenes and alkynes, followed by rearrangement of the intermediate 1,2-isomer, **IV$^{R,R'}$** (Scheme 1d).[33] Once again, the isomerisation can be prevented by starting from a cyclic diborene. Finally, we have reported the synthesis of a nickel(0) complex capped by a 2π-aromatic η^4-1,3-dihydro-1,3-diborete (**VI**), which is formed by a complex rearrangement of an N-heterocyclic carbene (NHC)-stabilised 1,2-divinyldiborene upon reaction with $Ni(cod)_2$ (cod = 1,5-cyclooctadiene, Scheme 1f).[34]

In contrast, the isolation of doubly Lewis-base-stabilised 1,2- and 1,3-diboretes, which are isoelectronic with cyclobutadiene, is significantly more challenging, as their 4π electrons make them formally antiaromatic (Scheme 2a). Efforts by our group to synthesise diboretes from the [2+2] cycloaddition of NHC-stabilised diborynes and alkynes resulted in complex rearrangement, intramolecular C–H activation, and NHC ring expansion reactions of the putative 1,2-diborete intermediates.[35] The [2+2] cycloaddition of 2-butyne with a cyclic alkyl(amino)carbene (CAAC)-stabilised diboron analogue, however, provided the stable, puckered 1,3-diborete **IX**, presumably via the 1,4-diborete intermediate **VIII** (Scheme 2b).[36] Like its cyclobutadiene analogue,[37-40] **IX** is a biradical species, its two unpaired electrons being delocalised over the B–(C–N)$_{CAAC}$ π bonds, effectively leaving only 2π electrons in the central C_2B_2 ring, which thus becomes slightly aromatic. As with dihydrodiboretes, annelation of the diborete C=C moiety with a rigid backbone prevents rearrangement of the 1,2- to the 1,3-diborete, thus enabling the isolation of the first 1,2-diborete, the naphthodiborete **XI**, by our group in 2022.[41]

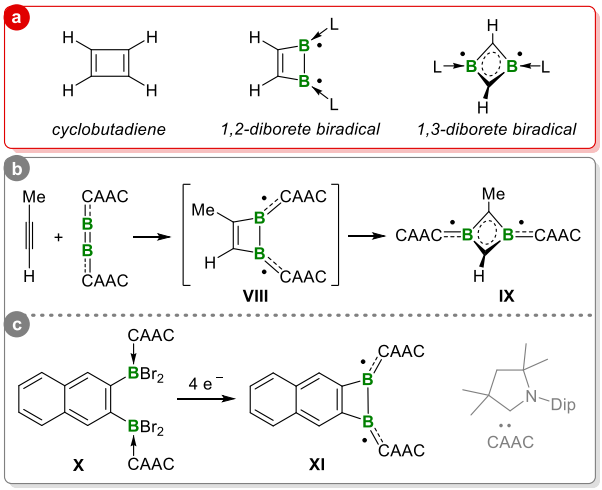

Scheme 2. Synthetic routes to the 1,2- and 1,3-isomers of diboretes.

In naphthodiborete **XI**, the strongly σ-donating and π-accepting CAAC ligands are key to stabilising the otherwise 4π-antiaromatic C_2B_2 ring by favouring a biradical structure,[42,43] with a B–B single bond and two unpaired electrons delocalised over the B–(C–N)$_{CAAC}$ π bonds. Compound **XI** reacts like a strained cyclic diborene, undergoing a [2+1] cycloaddition with phenyl azide, or like a bis(borylene), undergoing adduct formation with CO at each of the two boron centres to yield the naphthalene-bridged bis((CAAC,CO)-borylene) **XI(CO)$_2$**. Further, reversible two-electron reduction yields the dianionic 1,2-diboretes **[XI]$^{2-}$**, which display B=C$_{CAAC}$ double bonds.[41]

Herein, we present our investigations into the benzo-fused analogue of **XI** to study the influence of the aromatic fused backbone and the carbene ligand on the synthesis, stability, and reactivity of the resulting fused 1,2-diboretes.

Results and Discussion

Synthesis and structures of bis(dihaloboryl)benzene precursors

In our hands, Kaufmann's synthesis of the 1,2-bis(dichloroboryl)benzene precursor **1** from BCl_3 and 1-dichloroboryl-2-trimethylsilylbenzene (**XII**)[44] systematically yielded the undesired 9,10-dichloro-9,10-dihydro-9,10-diboraanthracene (**XIII**) and only small amounts (< 10%) of **1** (Scheme 3a). While Kaufmann had reported that the thermolysis of **XII** to **XIII** required 12 h at 135 °C in

hexachlorobutadiene,[45] we observed the formation of **XIII** even at 60 °C in the dilute gas phase under argon atmosphere. The formation of **XII** was finally successfully suppressed by using 3 equiv. of BCl_3 and performing the reaction in the gas phase at 95 °C under static vacuum (Scheme 3b). Distillation (b.p. 52 °C at $8.5 \cdot 10^{-2}$ mbar) yielded **1** as a viscous colourless oil in 91% yield. NMR-spectroscopic analysis, however, showed that **1** (δ_{11B} = 56.7 ppm) was systematically contaminated by small amounts (5-9%) of its 1,3 isomer **2**, which could not be separated by either chromatography or fractional distillation. Based on calculations by Zhao and coworkers on the reaction of trimethylsilylbenzene with BX_3 (X = Cl, Br),[46] we postulate that **2** is formed via *ortho*-S_EAr, generating the intermediate (2,6-bis(dichlorborylphenyl))trimethylsilane and HCl, which react to yield **2** and $ClSiMe_3$.

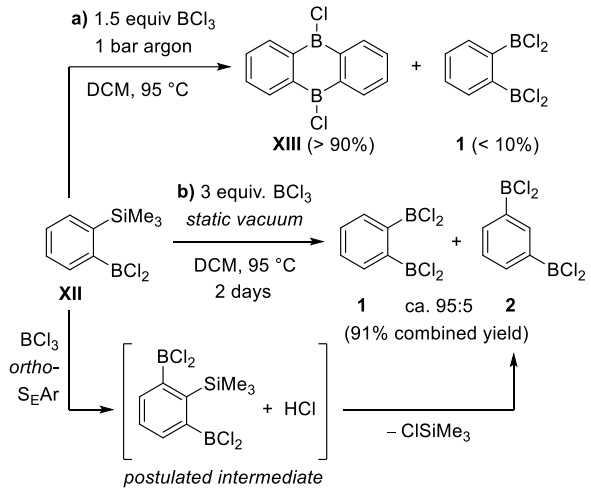

Scheme 3. Optimised synthesis of **1**. The static vacuum is created by condensing BCl_3 gas into the thick-walled Schlenk flask containing **XII** at –173 °C, then applying a high vacuum to the flask prior to sealing it and heating the mixture at 95 °C.

The addition of 2 equiv. I*i*Pr (= 1,3-di*iso*propylimidazol-2-ylidene) or CAAC to freshly distilled **1** (containing 5-9% of **2**) yielded the adducts **3-I*i*Pr** and **3-CAAC**, respectively (Scheme 4). While **3-I*i*Pr** could not be separated from its 1,3-isomer **4-I*i*Pr** (ca. 6%) due to their similar solubilities, **3-CAAC** could be isolated cleanly by washing with benzene, in which its 1,3-isomer **4-CAAC** (ca. 8%) is soluble. **3-I*i*Pr** and **3-CAAC** both present ^{11}B NMR resonances around 4 ppm. **3-CAAC** was only soluble in CH_2Cl_2, in which it rapidly underwent chloride abstraction and protonolysis to the ionic species **5** (δ_{11B} = 14 (br) ppm; δ_{1H} = 14.26 (s, $[HCl_2]^-$) ppm) and $[CAACH]^+$ (δ_{1H} = 11.35 (s, NC*H*) ppm).[47]

Compounds **3-I*i*Pr**, **3-CAAC**, **4-CAAC** and **5**, were analysed by single-crystal X-ray diffraction (Figure 1). The solid-state structures of the twofold adducts **3-I*i*Pr** and **3-CAAC** display an unexpected difference in their geometries. Whereas the benzo backbone in **3-I*i*Pr** is relatively planar (absolute values of torsion angles |C–C–C–C| ≤ 3.1(7)°) and nearly perpendicular to the NHC rings (ca. 84 and 88°), the greater steric profile of the two CAAC ligands in **3-CAAC** induce a significant twist in the benzo backbone ($|C–C–C–C|_{max}$ = 10.0(7)°) and a rotation of the carbene planes relative to the benzo ring (ca. 64°) to avoid steric clashes. In contrast, the benzo backbone of the 1,3 isomer **4-CAAC** is planar (|C–C–C–C| ≤ 1.4(2)°) as the two CAAC ligands are sufficiently removed from one another to avoid steric clashes.

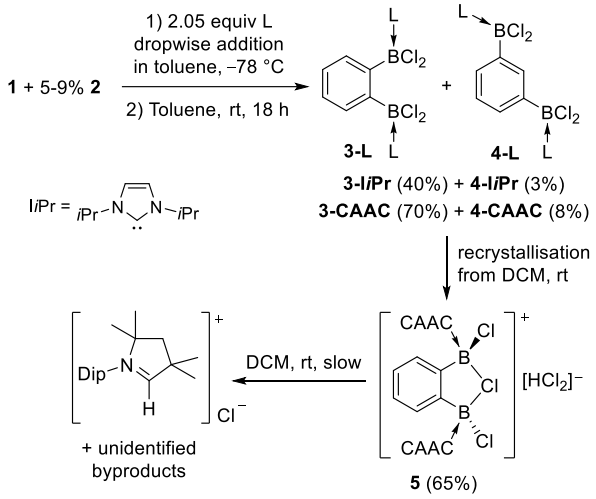

Scheme 4. Synthesis of NHC and CAAC adducts of **1**. DCM = dichloromethane.

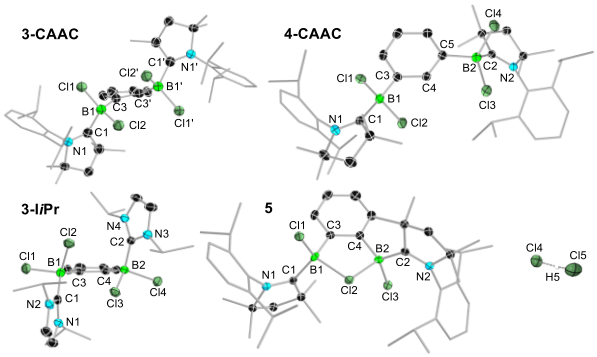

Figure 1. Solid-state structures of **3-CAAC**, **4-CAAC**, **3-I*i*Pr** and **5**. Atomic displacement ellipsoids at 50%. Ellipsoids of ligand periphery and hydrogen atoms omitted for clarity except for the HCl_2^- proton H5.

The solid-state structure of the cationic bis(borane) **5** displays a slightly unsymmetrically bridging chloride ($B–Cl_{bridge}$ = 2.015(3), 2.050(3) Å) and a quasi-planar benzo backbone (|C–C–C–C| ≤ 3.8(4)°), as well as an unusual $[Cl–H–Cl]^-$ counteranion (H–Cl 1.44(4) and 1.71(4) Å, Cl–H–Cl 174(4)°, hydrogen atom localised in the difference Fourier map and freely refined), resulting from DCM-derived HCl and chloride abstraction from **3-CAAC**. The $[HCl_2]^-$ anion was first observed in 1958 by powder diffraction of $[NMe_4][HCl_2]$,[48] and characterised in 1970 by single-crystal X-ray crystallography.[49] The unsymmetrical localisation of its hydrogen atom (avg. H···Cl 1.38 and 1.83 Å) and non-linearity (avg. Cl–H–Cl 171°) was only confirmed in 1981,[50] thereby ending a long-standing controversy about its structure.[51] Owing to the cyclic C_2B_2Cl motif, the distance between the two boron atoms in **5** (3.033(4) Å) is significantly shorter than in **3-CAAC** (3.571(8) Å), thus predisposing **5** to more facile B–B bond-forming reduction.

Reduction behaviour of 3-L

The reduction of **3-I*i*Pr** in THF with a large excess of Li sand proceeded via successive colour changes, first to green and then to red, over the course of 1 h. The ^{11}B NMR spectrum of the reaction mixture showed selective conversion to a single species with two broad resonances at 39.9 and 12.9 ppm, respectively. The product was identified by NMR spectroscopy and high-resolution mass spectrometry as the fused tricyclic compound **6** (Scheme 5). The ^{11}B NMR resonances of **6** match those reported by Kinjo for a similar 1,3-diborole structural motif (δ_{11B} = 38.2, 13.2 ppm).[52]

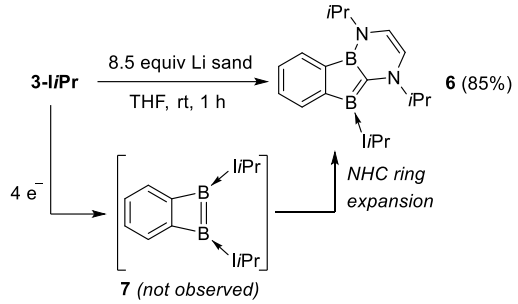

Scheme 5. Reduction of **3-I*i*Pr**.

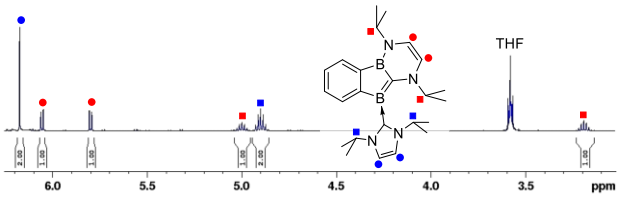

Figure 2. Annotated ^{1}H NMR spectrum of **6** in the 3-6.5 ppm region.

The ^{1}H NMR spectrum of **6** shows four inequivalent multiplets (1:1:1:1) for the protons of the now unsymmetrically substituted benzo backbone (δ_{1H} = 7.88, 7.38, 7.12 and 6.69 ppm), as well as the typical splitting pattern of one ring-expanded I*i*Pr ligand (marked in red in Figure 2), and one intact I*i*Pr ligand (marked in blue in Figure 2). The alkylideneborane and I*i*Pr-carbene ^{13}C NMR resonances, broadened by coordination to the quadrupolar boron nuclei, were detected by heteronuclear multiple bond correlation (HMBC) at 143.9 and 164.0 ppm, respectively.

Compound **6** is likely formed by the NHC-ring-expanding B=B bond activation of the doubly I*i*Pr-stabilised benzodiborete **7** – presumably the green intermediate observed at the start of the reaction – in a similar manner to the NHC ring expansion observed in NHC-stabilised diboranes(4).[53-55] Attempts to isolate this diborete by carrying out the reaction at –78 °C failed and resulted only in the isolation of **6**. The lower stability of diborete **7** compared to the CAAC-stabilised analogue **XI** is likely not solely owed to the lower steric protection afforded by I*i*Pr, but also to its significantly lower π-acceptor ability. This leaves the 1,2-diborete ring of **7** antiaromatic, and thus more reactive than its CAAC analogue **XI**, in which the π-electron density is delocalised as two unpaired electrons over the exocyclic B–(C–N)$_{CAAC}$ moieties, rendering the diborete ring effectively 2π-aromatic.[41]

The cyclic voltammogram of the ionic doubly CAAC-stabilised complex **5** in DCM showed five successive reductions at −0.81, −1.22, −1.83, −2.29 and −2.52 V, out of which only the redox event at −1.22 V is reversible (Figure 3).‡ Given the relatively clear separation of each of these electrochemical reductions, a stepwise chemical reduction of **5** or **3-CAAC** seemed achievable.

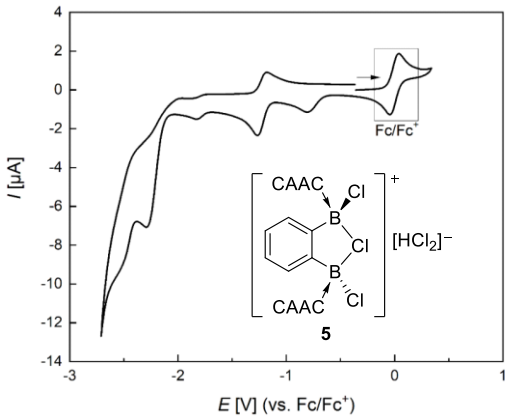

Figure 3. Cyclic voltammogram of **5** in DCM (electrolyte: [*n*Bu$_4$N][PF$_6$]), referenced to the ferrocene/ferrocenium (Fc/Fc$^+$) redox couple.

The one-electron reduction of **3-CAAC** to the pale-yellow radical **8** was achieved using 0.9 equiv. KC_8 (Figure 4a). The EPR spectrum of the reaction mixture showed a five-line signal at g_{iso} = 2.0038, which was fitted to a hyperfine splitting pattern of a(^{14}N, 2N) = 17.5 MHz, a(^{10,11}B, 2B) = 2.4 MHz, and a(^{35,37}Cl, 1Cl) = 4.6 MHz (Figure 4c). The observation that both nitrogen and boron nuclei feature identical hyperfine coupling constants, with one chloride participating in the coupling, initially suggests a symmetrical structure for **8**. However, computational analyses (*vide infra*) indicate that the unpaired electron is not symmetrically delocalised over a chloride-bridged π framework, but that the symmetrical EPR spectrum instead reflects a dynamic process involving Cl migration from one boron atom to the other. Attempts to crystallise **8** yielded colourless crystals of its hydrogen abstraction product **8-H** (Figure 4b), in which one CAAC ligand has been protonated at C3 and is now covalently bonded to B1 (B1–C3 1.616(2) Å), while the other remains a neutral donor ligand (B2–C4 1.585(3) Å) and the chloride bridges asymmetrically in a B2–Cl2→B1 fashion (B2–Cl2 1.9819(18), B1–Cl2 2.0792(19) Å).

The reduction of **3-CAAC** with 2.2 equiv. Na sand in diethyl ether afforded a brown solution of the diradical **9** (Figure 4a). The EPR spectrum of the reaction mixture (Figure 4d) showed a very broad symmetrical signal at g_{iso} = 2.0028, which could be

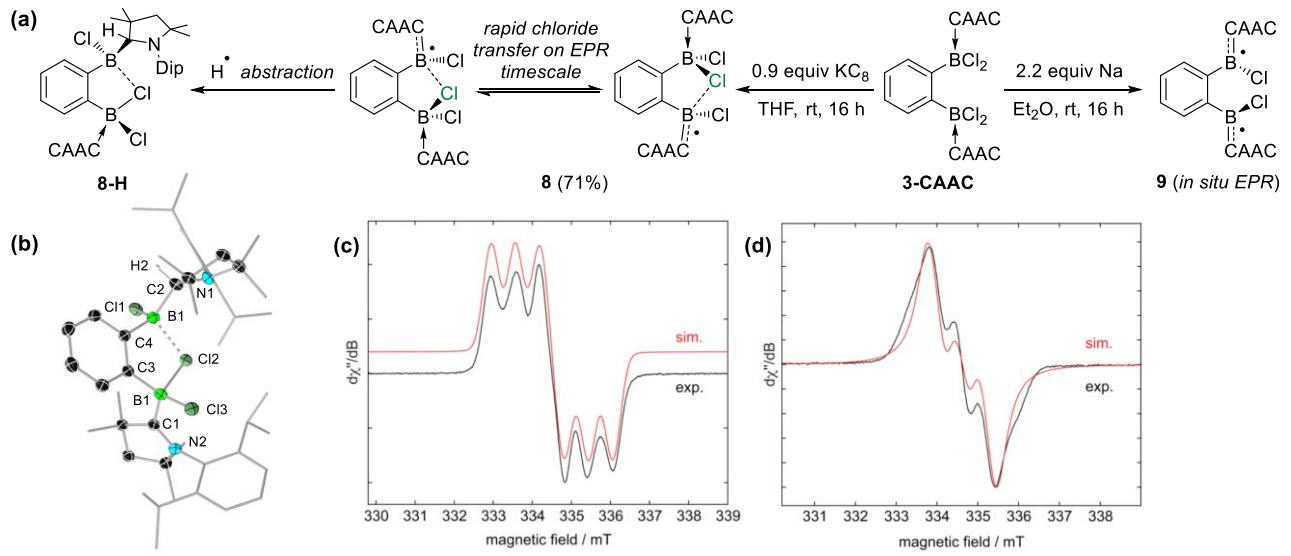

Figure 4. (a) *In-situ* generation of radical **8**, undergoing rapid intramolecular chloride transfer, and its decomposition to **8-H**. **(b)** Solid-state structure of **8-H**. Atomic displacement ellipsoids at 50%. Ellipsoids of ligand periphery and hydrogen atoms omitted for clarity except for H3. **(c)** Experimental (black) and simulated (red) solution EPR spectrum of **8** in THF at rt (g_{iso} = 2.0038). Parameters for best-fit simulation: $a(^{14}N, 2N)$ = 17.5 MHz, $a(^{10,11}B, 2B)$ = 2.4 MHz, $a(^{35,37}Cl, 1Cl)$ = 4.6 MHz. **(d)** Experimental (black) and simulated (red) solution EPR spectrum of **9** in Et_2O at rt (g_{iso} = 2.0028). Parameters for best-fit simulation: $a(^{14}N, 2N)$ = 16.5 MHz, $a(^{10,11}B, 2B)$ = 3.7 MHz.

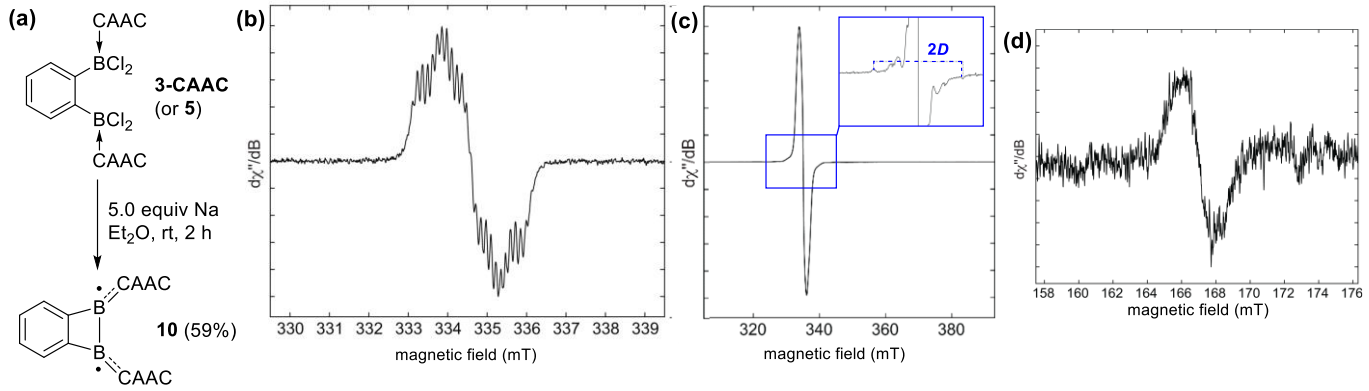

Figure 5. (a) Synthesis of the benzodiborete biradical **10**. **(b)** Experimental solution EPR spectrum of **10** in Et_2O at rt (g_{iso} = 2.0030). **(c)** Experimental powder EPR spectrum of **10** at rt (g_{iso} = 2.0030). Inset in blue frame: magnification of the 328-338 mT region highlighting the zero-field splitting (D = 840 MHz). **(d)** Half-field signal of the experimental powder EPR spectrum of **10** at rt.

fitted to a hyperfine splitting pattern of $a(^{14}N, 2N)$ = 16.5 MHz and $a(^{10,11}B, 2B)$ = 3.7 MHz, the latter being somewhat larger than in [(CAAC)BClDur]• ($a(^{10,11}B)$ = 1.5 MHz; Dur = 2,3,4,5-tetramethylphenyl).[56] The slight broadening of the signal, which could not be satisfactorily modelled, may result from the existence of several atropisomers of **9** in solution, also observed in the structurally related naphthalene analogue **XI(CO)$_2$**.[41]

In the presence of 5 equiv. Na in diethyl ether, **3-CAAC** and **5** both underwent a four-electron reduction yielding the red-coloured biradical benzodiborete **10** (Figure 5a). Complex **10** proved much less stable than the naphthodiborete **XI**,[41] decomposing upon solvent removal or prolonged storage in solution. Small amounts of red single crystals of **10** could be isolated by rapid evaporation of a saturated Et_2O solution in the glovebox, enabling its structural characterisation (see the **X-ray crystallography** section below). The room-temperature EPR spectrum of **10** revealed a multiline signal (Figure 5b), generated by hyperfine coupling to the two $^{10/11}B$ nuclei of the B–B unit, the two ^{14}N nuclei of the CAAC ligands, and the ^{1}H nuclei of the benzo bridge, suggesting some spin delocalisation over the latter (see the **DFT calculations** section below). The spectrum could not be satisfactorily simulated due to the complexity of the overlapping couplings. The biradical nature of **10** was confirmed by a powder EPR spectrum (Figure 5c), which provided a signal at g_{iso} = 2.0030, a zero-field splitting parameter D of ca. 31 mT (840 MHz), and a weak but clear forbidden Δm_S=2 half-field transition (Figure 5d). Using the point-dipole approximation, the distance r between the two unpaired spins is estimated as ca. 4.5 Å, which is slightly longer than that observed in the naphthodiborete **XI** (4.33 Å) and the distance between the two carbene centres in the solid-state structure of **10** (C3···C4 4.268(3) Å, see Figure 6).

Like its naphtho-fused analogue **XI**,[41] diborete **10** can undergo a further two-electron reduction. Thus, the

overreduction of **3-CAAC** (or **5**) with 8.5 equiv. of Li, Na or K yielded the corresponding dianions, which were isolated as red to brown crystals by recrystallisation from THF (**11-Li**), Et_2O (**11-Na**), and toluene/pentane (**11-K**, Scheme 6). Their ^{11}B NMR spectra all show a broad resonance in the 22-26 ppm region, similar to that of the dianionic naphthodiborete **[XI]$^{2-}$** ($\delta_{11B} \approx 25$ ppm).[41] While **11-Li** and **11-K** proved too sensitive for isolation in sufficient quantities for full characterisation, **11-Na** was isolated as the double Et_2O adduct in 87% yield. Its ^{13}C NMR $C_{CAAC=B}$ boraalkene resonance, detected by HMBC, appears at 164.2 ppm, ca. 50 ppm upfield-shifted from the $C_{carbene}$ resonance of the precursor **5** (δ_{13C} = 211.8 ppm), which reflects the strong π backbonding from the boron centres to the CAAC ligands.

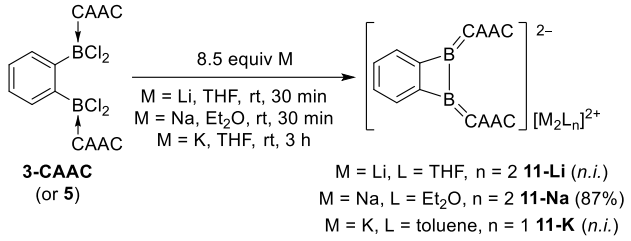

Scheme 6. Overreduction of **3-CAAC** (or **5**) to the dianions **11^{M}** (M = Li, Na, K).

The reduction of **5** with 5 equiv. Li in THF under a CO atmosphere did not proceed as selectively as that of its naphthalene analogue **XI**. While the latter selectively yielded the doubly (CAAC,CO)-stabilised naphtho-bis(borylene) **XI(CO)$_2$** (δ_{11B} = −9.6 ppm),[41] ^{11}B NMR spectra of the red-brown reaction mixture consistently showed two resonances at –2.4 and –10.1 ppm, which were identified by X-ray crystallographic analysis as the benzo[*d*][1,3]diborol-2-one **12** and the doubly (CAAC,CO)-stabilised benzo-bridged bis(borylene) **13**, respectively (Scheme 7a). To the best of our knowledge, **12** is the first example of a 1,3-diborol-2-one. It is likely formed through trapping of CO by the *in-situ*-generated biradical **9**, similarly to the reaction of our CAAC-stabilised 9,10-diboraathracene biradical with CO.[57]

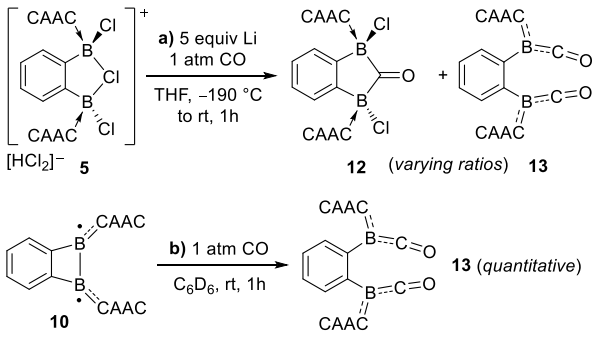

Scheme 7. Reduction of **5** under a CO atmosphere.

Efforts to target **12** or **13** selectively via this route by changing the reaction conditions (solvent, temperature, stoichiometry, pressure, time), or to separate them by recrystallisation failed, as they systematically cocrystallised in the same asymmetric unit (see the **X-ray crystallography** section below). The ^1H NMR spectrum of the product mixture only showed extremely broad resonances, indicative of fluctional processes, probably due to hindered rotation of the CAAC ligands. These could not be resolved by low- or high-temperature NMR spectroscopy. The bis(borylene) **13** was accessed selectively by submitting the diradical to an atmosphere of CO (Scheme 7b). Its ^{11}B NMR spectrum in C_6D_6 shows two distinct resonances at −11.2 and –12.2 ppm, likely corresponding to atropisomers, in which the CAAC ligand may be rotated either so that its Dip substituent points to the same side as the CO ligand or towards the benzo backbone, with which it likely features an edge-to-face CH/π interaction, as observed in the naphthodiborete **XI**.[41] Once more, the hindered rotation of the CAAC ligands about the B–C_{CAAC} multiple bonds causes severe broadening in the ^1H and ^{13}C NMR spectra of **13**, preventing their full NMR-spectroscopic characterisation. The solid-state IR spectrum of **13** shows two C=O stretching bands at 1978 and 1969 cm^{-1}, similar to the naphtho-bridged bis(borylene) **XI(CO)$_2$** (ν(C=O) = 1976, 1962 cm^{-1}).[41] Efforts to obtain the 1,3-diborol-2-one **12** selectively by first generating the bis(boryl) biradical **9** *in situ* prior to exchange of the argon with a CO atmosphere failed, due to the high sensitivity of **9**.

X-ray crystallography

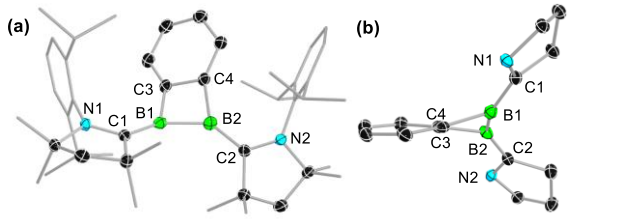

Figure 6. (a) Top view of the solid-state structure of **10**. Atomic displacement ellipsoids at 50%. Ellipsoids of ligand periphery and hydrogen atoms omitted for clarity. **(b)** Side view of the solid-state structure of **10**. Atomic displacement ellipsoids at 50%. Dip and Me substituents omitted for clarity.

The solid-state structure of **10** shows a highly twisted benzodiborete (Figure 6a,b) with average endocyclic torsion angles (absolute values) of 7.1° and 22.0° for the benzo and diborete rings, respectively (Table 1). In comparison, the naphthodiborete **XI** is significantly less twisted, with average endocyclic torsion angles (absolute values) of 6.6 and 19.1° for the benzo and diborete rings, respectively, presumably owing to the higher rigidity of the naphthalene backbone.[41] As in **XI**, the geometry of the boron centres in **10** also deviates from planarity (Σ∠B 354.74(19), 354.94(29)°) and the Dip substituents of both CAAC ligands point towards the benzo backbone (N1–C1–B1–C3 24.3(4), N2–C2–B2–C4 16.7(4)°). The B–B bond length of 1.710(3) Å is comparable to that in **XI** (1.701(5) Å), and thereby essentially a single bond, like that found in the diboron biradicals [(CAAC)B(EPh)]$_2$ (E = S, Se; B–B 1.700(4)-1.728(2)Å).[58] Furthermore, the B–C_{CAAC} bonds (1.523(3), 1.534(3) Å) display some double bond character, as is usually observed in CAAC-stabilised boryl radicals.[56,58-60]

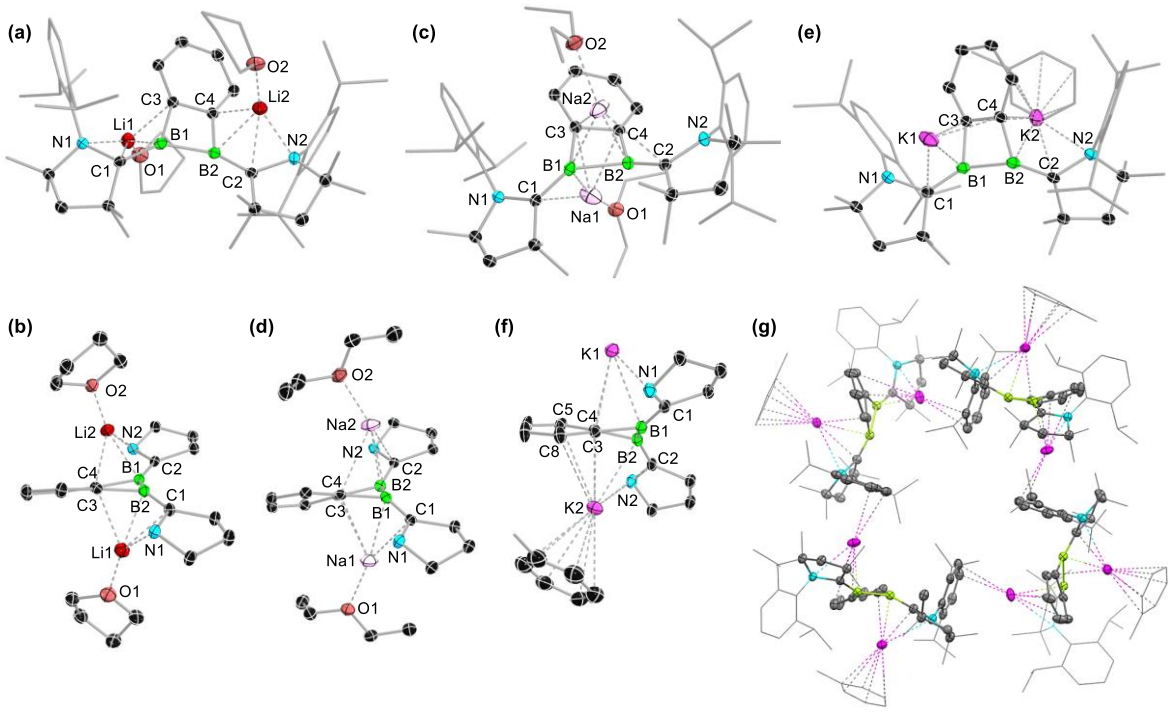

Figure 7. Solid-state structures of **(a,b) 11-Li**, **(c,d) 11-Na** and **11-K** (**(e,f)** monomeric unit and **(g)** tetrameric arrangement). Atomic displacement ellipsoids at 50%. Ellipsoids of ligand periphery and hydrogen atoms omitted for clarity. Metal-ligand interactions represented as dashed bonds. Side views **(b,d,f)**: Dip and Me substituents omitted for clarity.

Table 1. Selected bond lengths (Å), bond and torsion angles (°, absolute values) for the solid-state structures of **3-CAAC**, **5**, **8-H**, **10**, **11**-M (M = Li, Na, K), **12** and **13**. Ω_{C2B2} = endocyclic diborete torsion angles, Ω_{benzo} = endocyclic benzo torsion angles.

	3-CAAC[a,b]	**5**[b]	**8-H**[b]	**10**	**11-Li**	**11-Na**	**11-K**	**12**[a,c]	**13**[a,c]
B1–B2	3.571(8)	3.033(4)	3.052(3)	1.710(3)	1.805(2)	1.870(2)	1.808(3)	2.772(5)	3.315(5)
C3–C4	1.413(7)	1.403(4)	1.411(2)	1.417(3)	1.437(2)	1.443(2)	1.445(2)	1.416(6)	1.431(6)
C3–B1	1.616(7)	1.593(4)	1.585(3)	1.587(3)	1.6135(19)	1.601(2)	1.599(3)	1.593(5)	1.606(5)
C4–B2	–	1.581(4)	1.597(2)	1.586(3)	1.6209(19)	1.607(2)	1.599(3)	–	–
C1–B1	1.658(7)	1.658(7)	1.616(2)	1.523(3)	1.471(2)	1.476(2)	1.463(3)	1.611(5)	1.501(5)
C2–B2	–	1.645(4)	1.658(2)	1.534(3)	1.474(2)	1.479(2)	1.464(3)	–	–
B1–Y	1.893(6)	2.015(3)	2.0792(19)	–	–	–	–	1.737(5)	1.506(6)
B2–Y	1.893(6)	2.050(3)	1.9819(18)	–	–	–	–	–	–
C3–B1–B2	–	–	–	82.43(16)	83.19(10)	81.55(10)	81.92(13)	–	–
B1–B2–C4	–	–	–	83.08(16)	82.82(10)	81.48(10)	82.96(13)	–	–
B2–C4–C3	–	120.8(2)	119.86(14)	92.57(17)	95.88(11)	96.37(12)	95.85(14)	–	–
C3–C4–B1	122.1(4)	120.4(2)	122.22(15)	93.32(17)	95.99(11)	96.77(12)	94.60(14)	126.4(3)	125.93(18)
Σ∠B1	–	–	–	354.74(19)	356.29(13)	352.88(13)	355.38(17)	–	357.9(3)
Σ∠B2	–	–	–	354.94(20)	357.55(13)	352.33(14)	350.76(17)	–	–
$\lvert\Omega_{C2B2}\rvert$	–	–	–	19.8(1) to 23.8(2)	9.79(9) to 12.3(1)	13.1(1) to 17.0(1)	14.6(1) to 18.2(1)	–	–
$\lvert\Omega_{benzo}\rvert$	2.3(8) to 15.4(7)	0.7(4) to 3.8(5)	0.4(3) to 4.0(2)	0.7(3) to 10.8(3)	0.4(2) to 9.1(2)	1.7(2) to 17.8(2)	0.6(3) to 13.0(3)	0.1(5) to 0.3(5)	0.3(5) to 1.2(5)
|C3–B1–C1-N1|	150.8(5)	130.3(3)	162.3(2)	24.3(4)	0.2(2)	9.1(3)	12.6(3)	129.2(3)	168.6(3)
|C4–B2–C2-N2|	–	152.4(2)	165.9(2)	16.7(4)	1.0(2)	8.9(3)	9.1(3)	–	–

[a] The structure is C_2-symmetric; [b] Y = Cl2; [c] Y = C5.

In the three overreduced diborete complexes **11-M**, the nature of the cation and the crystallisation solvent has a strong influence on the solid-state structure (Table 1). All three complexes feature a twisted, doubly CAAC-stabilised benzodiborete sandwiched between two alkali metal cations featuring different interaction modes with the dianion, depending on the nature of the metal centres. Whereas **11-Li** and **11-Na** crystallise as monomers (Figure 7a-d), in which each of the two metal cations is stabilised by a THF and Et_2O molecule, respectively, **11-K** crystallises as a cyclic tetramer

(Figure 7e-g), in which K2 is stabilised by π interaction with a toluene molecule while K1 links to the adjacent monomeric unit through π interaction with its Dip substituent. In **11-Li**, each lithium cation coordinates to the π system of the nearest N-C_{CAAC}-B-C_{benzo} moieties (Li···N ca. 2.06, Li···C_{CAAC} ca. 2.14, Li···B ca. 2.24, Li···C_{benzo} 2.33 Å), one above and one below the benzodiborete plane. In **11-Na**, the sodium cations sit nearly centrally one above and one below the diborete ring, each featuring an additional interaction with the nearest B=C_{CAAC} π bond (Na···C_{CAAC} ca. 2.76, Na···B ca. 2.50-2.87, Na···C_{benzo} 2.65-2.92 Å). In the monomeric unit of **11-K**, the toluene-stabilised potassium cation K2 coordinates to the π system of the N2-C2-B2 moiety (K2···N2 3.0436(17), K2···C2 2.9627(19), K2···B2 2.915(2) Å), and features an additional π interaction with the C8-C3-C4-C5 half of the benzo ring (K2···C8 3.397(2), K2···C3 2.9573(18), K2···C4 2.7926(18), K2···C5 3.355(2) Å), whereas K1, which bridges between two adjacent monomeric units of **11-K**, interacts with the π system of the C1-B1-C3-C4 moiety (K1···C1 3.0927(17), K1···B1 2.916(2), K1···C3 2.9231(18), K1···C4 3.0128(18) Å). These varied π coordination modes reflect the relative hardness of the metal cations: being the hardest one, lithium favours π interactions with the polar C⎓B and C⎓N π bonds, whereas potassium, the softest, favours π interactions with the organic arene moieties. As in **10**, the geometry of the boron centres remain somewhat distorted from planarity (Σ∠B 350.76(17)-357.55(13)°), and the Dip substituents all point towards the benzo backbone (|N–C_{CAAC}–B–C_{benzo}| ≤ 12.6(3)°). The two-electron reduction of **10** results in significant lengthening of the B–B bond from 1.710(3) Å to ca. 1.80 Å in **11-Li** and **11-K** and even 1.870(2) Å in **11-Na**, the additional elongation in the latter resulting from the π coordination of the two sodium cations to the entire diborete ring. This relieves some strain in the diborete ring, which becomes less twisted than in **10** (|Ω_{C2B2}| = 19.8(1)-23.8(2)°), the twisting increasing, however, with the size of the alkali metal cation, from |Ω_{C2B2}| = 9.79(9)-12.3(1)° in **11-Li** to |Ω_{C2B2}| = 14.6(1)-18.2(1)° in **11-K**. In comparison, the B–B bond in **[XI][Li_2(thf)$_2$]** (1.772(6) Å), which is essentially isostructural to **11-Li**, is significantly shorter than in the latter (1.805(2) Å), as the rigidity of the naphthalene backbone restricts twisting in the diborete ring (|Ω_{C2B2}| = 7.6(3)-8.5(3)°).[41] Additionally, the B–C_{CAAC} bonds are shortened from partial double bonds in **10** (ca. 1.53 Å) to proper double bonds in **11-M** (1.463(3)-1.479(2) Å), as also observed in **[XI][Li_2(thf)$_2$]** (1.468(6), 1.473(6) Å).[41]

The carbonyl compounds **12** and **13** cocrystallised next to each other within the same asymmetric unit, each presenting C_2 symmetry (Figure 8). Compound **12** presents a virtually planar benzo[*d*][1,3]diborol-2-one core, in which the sp^3-boron atoms are coordinated by two purely σ-donating CAAC ligands (B1–C1 1.611(5) Å). The B1–C5 (1.737(5) Å) bond length is within the range observed for other cyclic carbonyl-bridged sp^3,sp^3-diboron systems (B–C 1.64-1.76), while the C5–O1 bond (1.127(6) Å) is significantly shorter than in these systems (C–O ca. 1.21 Å).[57,61,62] Compound **13** features two benzene-bridged tricoordinate borylene moieties deviating slightly from planarity (Σ∠B1 357.9(3)°), stabilised by donor-acceptor bonds to both the CAAC and CO ligands of virtually equal strength (C1–B1 1.501(5), B1–C5 1.506(6) Å). In contrast, the B–C_{CO} bonds in the naphthalene analogue **XI(CO)$_2$** are significantly shorter (ca. 1.47 Å) than the B–C_{CAAC} bonds (ca. 1.51 Å).[41] Conversely, the C5–O1 bond in **13** (1.085(4) Å) is significantly shorter than in **XI(CO)$_2$** (1.157(2), 1.160(2) Å). Furthermore, the benzene and boron planes in **13** are orthogonal (ca. 89°), whereas the naphthalene and boron planes in **XI(CO)$_2$** form a more acute angle of ca. 58°. Both CAAC ligands are rotated so that their Dip substituents point towards the CO moieties (|N1–C1–B1–C5| 6.5(5)°), whereas in the solid-state structure of **XI(CO)$_2$**, one Dip substituent points towards the CO ligand and the other towards the naphthalene backbone.

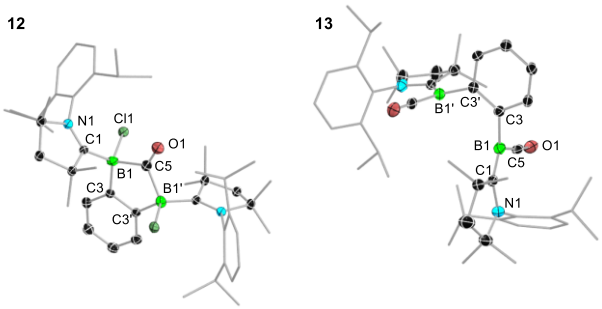

Figure 8. Solid-state structure of cocrystallised **12** and **13** as they appear in the asymmetric unit. Both compounds are C_2-symmetric. Atomic displacement ellipsoids at 50%. Ellipsoids of ligand periphery and hydrogen atoms omitted for clarity.

DFT calculations

To gain deeper insights into the electronic structure of the compounds, quantum chemical calculations were performed, using both density functional theory (DFT) and additional high-level multireference methods.

For the monoradical **8**, all attempts to obtain a minimum-energy structure for **8** with a symmetrically bridging chloride, as suggested by its solution EPR spectrum (Figure 4c), were unsuccessful, leading instead to an unsymmetrical structure with localised sp^3-borane and sp^2-boryl radical moieties (B1–(μ-Cl) 1.90 Å; B2···(μ-Cl) 3.01 Å). Constrained optimisations revealed that enforcing a symmetrical motif (see structure **8'** in the ESI) incurs an energy penalty of ca. 20 kcal mol^{-1}. The latter also represents an upper limit for the transition-state energy of Cl exchange between the two boron atoms, indicating that this migration is feasible at room temperature. Mayer bond order (MBO)[63] calculations indicate that, unlike in the symmetrical chloride-bridged cation **5**, in which both B–(μ-Cl) bonds have MBO values of 0.54, the bonding in **8**, with B–(μ-Cl) MBOs of 0.86 and 0.06, is more akin to that of the hydrogen abstraction product **8-H** (MBOs of 0.84 and 0.10). We suggest, therefore, that the identical EPR hyperfine coupling to both boron and nitrogen nuclei observed for **8** reflects a dynamic process involving Cl shuttling between the boron atoms on the EPR timescale, rather than a symmetrically Cl-bridged structure.

Further computations focused on compounds **9**-**11^{2-}**, with compound **11^{2-}** modelled as the bare dianionic benzodiborete system, explicitly excluding any countercations. The main findings, summarised in Figure 9, highlight the distinct

electronic structures of these systems. DFT single-point energy calculations at the ωB97X-D[64]/Def2-TZVP[65] level of theory, performed on geometries optimised at the ωB97X-D/Def2-SVP level, indicate that compound **9** has a triplet ground state, while compound **10** adopts an open-shell singlet (OSS) ground state. The calculated open-shell singlet-triplet (ST) gaps are –2.83 kcal mol^{-1} for **9** and +0.17 kcal mol^{-1} for **10**, where a negative value corresponds to a triplet ground state. High-level multireference calculations at the DLPNO-NEVPT2[66]/CASSCF(2,2)/Def2-TZVP level further refined these gaps to –3.26 and 0.08 kcal mol^{-1}, respectively, confirming the initial assignments. The electronic structure of **10** thus mirrors that of the naphthodiborete **XI**,[41] for which the predicted open-shell ST gaps were +0.08 kcal mol^{-1} at the DFT level and 1.5 kcal mol^{-1} based on multireference wavefunctions. For **10**, the small ST gap allows the higher triplet state to be thermally accessible at rt. Conversely, **9** has an ST gap that is too large to permit thermal population of the singlet state under typical conditions, including moderate heating. Finally, the dianion **11^{2-}** exhibits a closed-shell singlet (CSS) ground state, with its triplet state lying significantly higher in energy, at 40.4 kcal mol^{-1} above the singlet. As in the naphtho-fused analogues, most of the electron spin density of **9** and **10** resides on the B–C_{CAAC} π bonds and the nitrogen atoms of the CAAC rings, with no significant delocalisation through the C_2B_2 ring or the adjacent benzene ring.

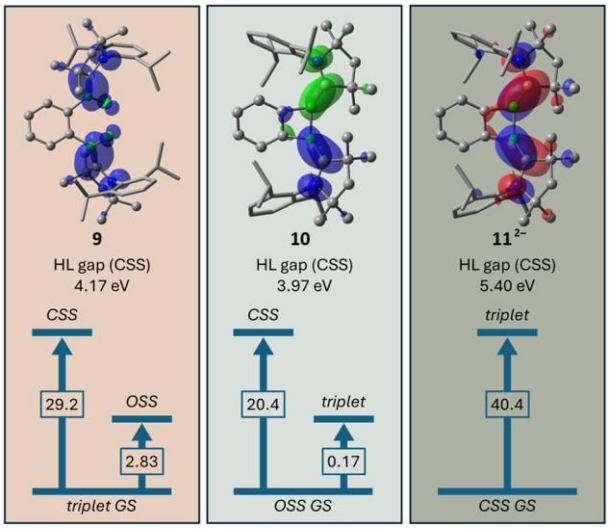

Figure 9. Summary of the DFT results obtained for compounds **9**-**11**. Top: Mulliken spin density plots of **9** and **10**, and HOMO of **11^{2-}** (hydrogen atoms omitted for clarity), with HOMO-LUMO (HL) gaps of the closed-shell singlet (CSS) structures. Isovalues for the spin densities: 0.003 a.u.; for the MO: 0.03 a.u. Bottom: energy differences (kcal mol^{-1}) between the CSS, open-shell singlet (OSS), and triplet states (GS = ground state). Calculations performed at the ωB97X-D/Def2-TZVP//ωB97X-D/Def2-SVP level of theory.

Finally, the aromatic character of the C_2B_2 ring of compound **10** was investigated by analysing the zz component of the nucleus-independent chemical shift ($NICS_{zz}$, Figure SX).[67-70] The $NICS_{zz}$(–1/1) values indicate a weakly 2π-aromatic system with –3.0 ppm for the OSS and –8.7 ppm for the triplet state, while the high-lying CSS state with 23.0 ppm corresponds to a 4π-antiaromatic system. These results are also commensurate with those of the naphthodiborete **XI** ($NICS_{zz}(-1/1)_{OSS}$ for the OSS: –3.8 ppm; for the triplet state: –7.8 ppm).[41]

Conclusions

In this work we have reported the synthesis of the second isolable 1,2-diborete, an analogue of cyclobutadiene, stabilised by strongly π-accepting CAAC ligands at the boron centres and fusion of the C=C bond to a rigid benzo backbone. The synthesis proceeds via twofold adduct formation of the precursor 1,2-bis(dichloroboryl)benzene (**1**) with CAAC, yielding compound **3-CAAC** or its cationic equivalent **5**, followed by four-electron reduction to the highly twisted benzodiborete **10**. In contrast, the four-electron reduction of the analogous I*i*Pr adduct resulted in the formation of a fused tricyclic structure (**6**), presumably a unstable antiaromatic benzodiborete intermediate (**7**), undergoing NHC ring expansion and B=B bond cleavage. The intermediate one-electron (boryl radical **8**) and two-electron reduction steps (bis(boryl) biradical **9**) were characterised by EPR spectroscopy. EPR-spectroscopic and computational analyses showed that diborete **10** has an open-shell singlet biradical ground state, a very small singlet-triplet gap, and thus a thermally accessible triplet state, as well as a small but non-negligible 2π-aromatic character. Further two-electron reduction of **10** with alkali metal reagents led to the isolation of the highly sensitive dianions **10-M** (M = Li, Na, K). Finally, reduction of **5** under CO atmosphere yielded a mixture of a unique 1,3-diborol-2-one (**12**) and the bis(CAAC,CO)borylene **13**, the latter also being accessible selectively by placing diborete **10** under a CO atmosphere.

On the one hand, these results essentially mirror those obtained for our previously reported naphthalene-based system (see Scheme 2c), albeit with a number of drawbacks. Firstly, the synthesis of the precursor **1** is less straightforward than that of **X**, requiring much harsher reaction conditions, and systematically yielding small amounts of inseparable byproducts. Secondly, compound **1**, its carbene adducts, and its reduction products are all significantly more sensitive than the corresponding naphthalene analogues towards decomposition. Finally, the experimental and computational data show little divergence between the benzo and naphtho congeners, except for the higher degree of twisting in the solid-state structure of the more flexible benzodiborete, and the observation of EPR hyperfine coupling to the protons of its benzo backbone.

On the other hand, the reduction of the I*i*Pr adduct **3-I*i*Pr** to **6**, which suggests the intermediate formation of the benzodiborete **7**, hints at the possibility of stabilising more electron-rich 1,2-diboretes using bulkier and slightly more π-accepting NHC ligands than I*i*Pr, less prone to ring expansion. These would be expected to display different reactivity to the CAAC derivatives as their 1,2-diborete ring are likely to have a more antiaromatic character.

Conflicts of interest

There are no conflicts to declare.

Acknowledgements

Financial support from the Deutsche Forschungsgemeinschaft is gratefully acknowledged (DFG project codes 466754611 and BR1149/22-2). L. E. thanks the Verband der Chemischen Industrie (VCI) for a Kekulé fellowship. This article is based upon work from the COST Action CA20129 - Multiscale Irradiation and Chemistry Driven Processes and Related Technologies (MultIChem), supported by COST (European Cooperation in Science and Technology).

Notes and references

‡ The neutral compound **3-CAAC** was not sufficiently soluble in polar solvents to obtain meaningful cyclovoltammetry data.

1 J.-J. Zhang, J. Ma and X. Feng, Precision Synthesis of Boron-Doped Graphene Nanoribbons: Recent Progress and Perspectives. *Macromol. Chem. Phys*., 2023, **224**, 2200232.
2 S. V. Sawant, A. W. Patwardhan, J. B. Josh and K. Dasgupta, Boron doped carbon nanotubes: Synthesis, characterization and emerging applications – A review. *Chem. Eng. J*., 2022, **427**, 131616.
3 S. K. Mellerup and S. Wang, Boron-doped molecules for optoelectronics. *Trends Chem.*, 2019, **1**, 77−89.
4 J. He, F. Rauch, M. Finze and T. B. Marder, (Hetero)arene-fused boroles: a broad spectrum of applications. *Chem. Sci*., 2021, **12**, 128−147.
5 M. Sindlinger, M. Ströbele, J. Grunenberg and H. F. Bettinger, Accessing unusual heterocycles: ring expansion of benzoborirenes by formal cycloaddition reactions. *Chem. Sci*., 2023, **14**, 10478–10487.
6 X. Su, T. A. Bartholome, J. R. Tidwell, A. Pujol, S. Yruegas, J. J. Martinez and C. D. Martin, 9-Borafluorenes: Synthesis, Properties, and Reactivity. *Chem. Rev*., 2021, **121**, 4147−4192.
7 X. Su, J. J. Baker and C. D. Martin, Dimeric boroles: effective sources of monomeric boroles for heterocycle synthesis. *Chem. Sci*., 2020, **11**, 126–131.
8 B. Su and R. Kinjo, Construction of Boron-Containing Aromatic Heterocycles. *Synthesis*, 2017, **49**, 2985−3034.
9 J. H. Barnard, S. Yruegas, K. Huang and C. D. Martin, Ring expansion reactions of anti-aromatic boroles. *Chem. Commun*., 2016, **52**, 9985−9991.
10 H. Braunschweig, I. Krummenacher and J. Wahler, Free Boroles: The Effect of Antiaromaticity on Their Physical Properties and Chemical Reactivity. *Adv. Organomet. Chem*., 2013, **61**, 1−53.
11 H. Braunschweig, M. A. Celik, T. Dellermann, G. Frenking, K. Hammond, F. Hupp, H. Kelch, I. Krummenacher, F. Lindl, L. Mailänder, J. H. Müssig and A. Ruppert, Scope of the Thermal Ring-Expansion Reaction of Boroles with Organoazides. *Chem. Eur. J*., 2017, **23**, 8006–8013.
12 M. Dietz, M. Arrowsmith and H. Braunschweig, CAAC-stabilised 9,10-diboraanthracene: an electronically and structurally flexible platform for small-molecule activation and metal complexation. *Dalton Trans.*, 2024, **53**, 449−453.
13 L. Zhang, M. Lei and Z. Cao, Hydroboration Reduction of CO_2 Catalyzed by a Doubly Reduced Arylborane: DFT Insight into Double Active-Site and CO_2 Self-Promoting Single Active-Site Mechanisms and Counterion Effects. *ACS Catal.*, 2024, **14**, 344–354.
14 C. Zhang, X. Liu, J. Wang and Q. Ye, A Three-Dimensional Inorganic Analogue of 9,10-Diazido-9,10-Diboraanthracene: A Lewis Superacidic Azido Borane with Reactivity and Stability. *Angew. Chem., Int. Ed*., 2022, **61**, e202205506.
15 S. Xu, L. A. Essex, J. Q. Nguyen, P. Farias, J. W. Ziller, W. H. Harman and W. J. Evans, Cooperative dinitrogen capture by a diboraanthracene/samarocene pair. *Dalton Trans*., 2021, **50**, 15000–15002.
16 M. Dietz, M. Arrowsmith, A. Gärtner, K. Radacki, R. Bertermann and H. Braunschweig, Harnessing the electronic differences between CAAC-stabilised 1,4-diborabenzene and 9,10-diboraanthracene for synthesis. *Chem. Commun.*, 2021, **57**, 13526–13529.
17 H. Budy, S. E. Prey, C. D. Buch, M. Bolte, H.-W. Lerner and M. Wagner, Nucleophilic borylation of fluorobenzenes with reduced arylboranes. *Chem. Commun*., 2022, **58**, 254–257.
18 S. E. Prey and M. Wagner, Threat to the Throne: Can Two Cooperating Boron Atoms Rival Transition Metals in Chemical Bond Activation and Catalysis? *Adv. Synth. Catal*., 2021, **363**, 2290−2309.
19 S. M. van der Kerk, P. H. M. Budzelaar, A. van der Kerk-van Hoof, G. J. M. van der Kerk and P. von Ragué Schleyer, Synthesis of Borirenes and Diboretenes — a Novel Class of 2π-Aromatic Compounds. *Angew. Chem., Int. Ed. Engl.*, 1983, **22**, 48.
20 M. Hildenbrand, H. Pritzkow, U. Zenneck and W. Siebert, Synthesis and Structure of a 1,3-Dihydro-1,3-diborete. *Angew. Chem., Int. Ed. Engl*., 1984, **23**, 371−372.
21 P. von Ragué Schleyer, P. H. M. Budzelaar, D. Cremer and E. Kraka, Puckered Structures of 1,3-Dihydro-1,3-diboretes and Bicyclobutane-2,4-dione: Nonplanar Hückel 2π-Electron Aromatic Molecules. *Angew. Chem., Int. Ed. Engl*., 1984, **23**, 374−375.
22 P. H. M. Budzelaar, K. Krogh-Jespersen, T. Clark and P. von Ragué Schleyer, J. *Am. Chem. Soc*., 1985, **107**, 2773−2779.
23 M. L. McKee, Ab Initio Study of Rearrangements on the $(CH)_2(BR)_2$, RH, and NH_2 Potential Energy Surfaces. *Inorg. Chem*., 2000, **39**, 4206−4210.
24 K. Krogh-Jespersen, P. von Ragué Schleyer, J. A. Pople and D. Cremer, Nonplanar structures of cyclobutadiene dications. *J. Am. Chem. Soc*., 1978, **100**, 4301−4302.
25 Y. Liu, I. B. Bersuker and J. E. Boggs, Pseudo Jahn–Teller origin of puckering in $C_4H_4^{2+}$, $Si_4H_4^{2+}$, and $C_4F_4^{2+}$ dications *Chem. Phys*., 2013, **417**, 26−29.
26 B. K. Paul, On the Aromaticity of Puckered Ions $C_4H_4^{2+}$ and $B_4H_4^{2-}$: Deciphering the Origin of Nonplanarity. *ChemSelect*, 2023, **8**, e202302373.
27 R. C. Wehrmann, H. Pues, A. Klusik and A. Berndt, 1,3-Dihydro-1,3-diboretes and Their Radical Anions. *Angew. Chem., Int. Ed. Engl*., 1984, **23**, 372−373.
28 M. Hildenbrand, H. Pritzkow and W. Siebert, 1,2-Bis(diisopropylamino)-1,2-dihydro-1,2-diboret. *Angew. Chem*., 1985, **97**, 769−770.
29 D. E. Kaufmann, R. Boese and A. Scheer, 1,2-Bis(diisopropylamino)-1,2-dihydro-1,2-benzodiboret - ein erstes thermisch stabiles 1,2-Dihydro-1,2-diboret. *Chem. Ber*., 1994, **127**, 2349−2351.
30 A. Krämer, H. Pritzkow and W. Siebert, Synthese und Struktur von 2,4,6,8-Tetrakis(diisopropylamino)-2,4,6,8-tetrabora-tricyclo-[3,3,0,$0^{3,7}$]-octan. *Z. Naturforsch*., 1989, **44b**, 96−98.
31 A. Krämer, H. Pritzkow and W. Siebert, Synthesis and Structure of a 1,2,5,6-Tetrahydro-1,2,5,6-tetraborocine. *Angew. Chem., Int. Ed. Engl*., 1988, **27**, 926−297.
32 R. A. Thornton and B. M. Lindley, Bonding and Reactivity of a Diborabutadiene Fe Complex Synthesized by Boron−Boron Bond Activation. *Organometallics*, 2023, **42**, 1454−1458.
33 L. Englert, U. Schmidt, M. Dömling, M. Passargus, T. E. Stennett, A. Hermann, M. Arrowsmith, M. Härterich, J. Müssig, A. Phillipps, D. Prieschl, A. Rempel, F. Rohm, K. Radacki, F. Schorr, T. Thiess, J. O. C. Jiménez-Halla and H. Braunschweig, Reactions of diborenes with terminal alkynes: mechanisms of ligand-controlled anti-selective hydroalkynylation, cycloaddition and C≡C triple bond scission. *Chem. Sci.*, 2021, **12**, 9506–9515.

34 A. Hermann, F. Fantuzzi, M. Arrowsmith, T. Zorn, I. Krummenacher, B. Ritschel, K. Radacki, B. Engels and H. Braunschweig, Oxidation, Coordination, and Nickel-Mediated Deconstruction of a Highly Electron-Rich Diboron Analogue of 1,3,5-Hexatriene. *Angew. Chem.*, *Int. Ed.*, 2020, **59**, 15717–15725.

35 T. Brückner, M. Arrowsmith, M. Heß, K. Hammond, M. Müller and H. Braunschweig, Synthesis of fused B,N-heterocycles by alkyne cleavage, NHC ring-expansion and C–H activation at a diboryne. *Chem. Commun.*, 2019, **55**, 6700–6703.

36 M. Arrowsmith, J. Böhnke, H. Braunschweig, M. A. Celik, C. Claes, W. C. Ewing, I. Krummenacher, K. Lubitz and C. Schneider, Neutral Diboron Analogues of Archetypal Aromatic Species by Spontaneous Cycloaddition. *Angew. Chem.*, *Int. Ed.*, 2016, **55**, 11271–11275.

37 A. Kostenko, B. Tumanskii, Y. Kobayashi, M. Nakamoto, A. Sekiguchi and Y. Apeloig, Spectroscopic Observation of the Triplet Diradical State of a Cyclobutadiene. *Angew. Chem., Int. Ed*., 2017, **56**, 10183–10187.

38 F. Fantuzzi, T. M. Cardozo and M. A. C. Nascimento, The Nature of the Singlet and Triplet States of Cyclobutadiene as Revealed by Quantum Interference. *ChemPhysChem*, 2016, **17**, 288–295.

39 J. I-C. Wu, Y. Mo, F. A. Evangelista and P. von Ragué Schleyer, Is cyclobutadiene really highly destabilized by antiaromaticity? *Chem. Commun*., 2012, **48**, 8437–8439.

40 A. Balkova and R. J. Bartlett, *J. Chem. Phys*., 1994, **101**, 8972–8987.

41 A. Gärtner, L. Meier, M. Arrowsmith, M. Dietz, I. Krummenacher, R. Bertermann, F. Fantuzzi and H. Braunschweig, Highly Strained Arene-Fused 1,2-Diborete Biradicaloid. *J. Am. Chem. Soc.*, 2022, **144**, 21363–21370.

42 M. Soleilhavoup and G. Bertrand, Cyclic (alkyl)(amino)carbenes (CAACs): stable carbenes on the rise. *Acc. Chem. Res.*, 2015, **48**, 256−266.

43 S. Kundu, S. Sinhababu, V. Chandrasekhar and H. W. Roesky, Stable cyclic (alkyl)(amino)carbene (cAAC) radicals with main group substituents. *Chem. Sci*., 2019, **10**, 4727−4741.

44 D. Kaufmann, Borylierung von Arylsilanen, II Synthese und Reaktionen silylierter Dihalogenphenylborane. *Chem. Ber.*, 1987, **120**, 901–905.

45 W. Schacht, D. Kaufmann, Thermolyse von Arylhalogenboranen; Synthese von 1,3-Dibora- und 1,3-Borasilaindanen. *J. Organomet. Chem*., 1987, **331**, 139-152.

46 C. S. Qiu, N. P. Qiu, C. Flinn, Y. Zhao, DFT mechanistic studies of boron–silicon exchange reactions between silyl-substituted arenes and boron bromides. *Phys. Chem. Chem. Phys*., 2023, **25**, 6714–6725.

47 R. Jazzar, R. D. Dewhurst, J.-B. Bourg, B. Donnadieu, Y. Canac and G. Bertrand, Intramolecular "Hydroiminiumation" of Alkenes: Application to the Synthesis of Conjugate Acids of Cyclic Alkyl Amino Carbenes (CAACs). *Angew. Chem., Int. Ed*., 2007, **46**, 2899–2902.

48 T. C. Waddington, The Preparation of Tetramethylammonium Hydrogen Dichloride and the Structure of the Hydrogen Dichloride Ion, HCl_2^-, *J. Chem. Soc.*, 1958, 1708–1709.

49 J. S. Swanson and J. M. Williams, Bichloride ion geometry in tetramethylammonium bichloride ($TMAHCl_2$): An X-ray diffraction study. *Inorg. Nucl. Chem. Lett*., 1970, **6**, 271–276.

50 D. Mootz, W. Poll, H. Wunderlich and H.-G. Wussow, Phosphonium-hydrogendichloride, II Drei Kristallstrukturen im Vergleich. *Chem. Ber*., 1981, **114**, 3499–3504.

51 D. G. Tuck, Structures and Properties of HX_2^- and HXY^- Anions. In *Progr. Inorg. Chem*. (ed. F. A. Cotton), 1968, **9**, 161-194, Interscience, New York.

52 W. Lu, Y. Li, R. Ganguly, and R. Kinjo, Crystalline Neutral Allenic Diborene. *Angew. Chem., Int. Ed*., 2017, **56**, 9829–9832.

53 S. Pietsch, U. Paul, I. A. Cade, M. J. Ingleson, U. Radius and T. B. Marder, Room Temperature Ring Expansion of N-Heterocyclic Carbenes and B–B Bond Cleavage of Diboron(4) Compounds. *Chem. Eur. J*., 2015, **21**, 9018–9021.

54 M. Eck, S. Würtemberger-Pietsch, A. Eichhorn, J. H. J. Berthel, R. Bertermann, U. S. D. Paul, H. Schneider, A. Friedrich, C. Kleeberg U. Radius and T. B. Marder, B–B bond activation and NHC ring-expansion reactions of diboron(4) compounds, and accurate molecular structures of $B_2(NMe_2)_4$, B_2eg_2, B_2neop_2 and B_2pin_2. *Dalton Trans*., 2017, **46**, 3661–3680.

55 T. Thiess, S. K. Mellerup and H. Braunschweig, B−B Cleavage and Ring-Expansion of a 1,4,2,3-Diazadiborinine with N-Heterocyclic Carbenes. *Chem. Eur. J*., 2019, **25**, 13572–13578.

56 P. Bissinger, H. Braunschweig, A. Damme, I. Krummenacher, A. K. Phukan, K. Radacki, S. Sugawara, Isolation of a Neutral Boron-Containing Radical Stabilized by a Cyclic (Alkyl)(Amino)Carbene. *Angew. Chem. Int. Ed.*, **2014**, *53*, 7360–7363.

57 C. Saalfrank, F. Fantuzzi, T. Kupfer, B. Ritschel, K. Hammond, I. Krummenacher, R. Bertermann, R. Wirthensohn, M. Finze, P. Schmid, V. Engel, B. Engels, H. Braunschweig, cAAC-Stabilized 9,10-diboraanthracenes—Acenes with Open-Shell Singlet Biradical Ground States. Christian Saalfrank, Dr. Felipe Fantuzzi, Dr. Thomas Kupfer, *Angew. Chem.*, *Int. Ed.*, 2020, **59**, 19338–19343.

58 J. Böhnke, T. Dellermann, M. A. Celik, I. Krummenacher, R. D. Dewhurst, S. Demeshko, W. C. Ewing, K. Hammond, M. Heß, E. Bill, E. Welz, M. Röhr, R. Mitrić, B. Engels, F. Meyer and H. Braunschweig, Isolation of diborenes and their 90°-twisted diradical congeners. *Nature Commun.*, 2018, **9**, 1197.

59 A. Deißenberger, E. Welz, R. Drescher, I. Krummenacher, R. D. Dewhurst, B. Engels and H. Braunschweig, A New Class of Neutral Boron-Based Diradicals Spanned by a Two-Carbon-Atom Bridge. *Angew. Chem.*, *Int. Ed.*, 2019, **58**, 1842–1846.

60 S. Hagspiel, M. Arrowsmith, F. Fantuzzi, A. Hermann, V. Paprocki, R. Drescher, I. Krummenacher and H. Braunschweig, Reduction of a dihydroboryl cation to a boryl anion and its air-stable, neutral hydroboryl radical through hydrogen shuttling. *Chem. Sci.*, 2020, **11**, 551–555.

61 A. Stoy, M. Härterich, R. D. Dewhurst, J. O. Jimenez-Halla, P. Endres, M. Eißelein, T. Kupfer, A. Deissenberger, T. Thiess and H. Braunschweig, Evidence for Borylene Carbonyl (LHB=C=O) and Base-Stabilized (LHB=O) and Base-Free Oxoborane (RB≡O) Intermediates in the Reactions of Diborenes with CO_2. *J. Am. Chem. Soc.*, 2022, **144**, 3376–3380.

62 A. Stoy, J. Böhnke, J.O.C. Jimenéz-Halla, R. D. Dewhurst, T. Thiess and H. Braunschweig, CO_2 Binding and Splitting by Boron–Boron Multiple Bonds. *Angew. Chem.*, *Int. Ed.*, 2018, **57**, 5947–5951.

63 I. Mayer, Bond order and valence indices: A personal account. *J. Comput. Chem*., 2007, **28**, 204–221.

64 J.-D. Chai and M. Head-Gordon, Long-range corrected hybrid density functionals with damped atom–atom dispersion corrections. *Phys. Chem. Chem. Phys.*, 2008, **10**, 6615.

65 F. Weigend and R. Ahlrichs, Balanced basis sets of split valence, triple zeta valence and quadruple zeta valence quality for H to Rn: Design and assessment of accuracy. *Phys. Chem. Chem. Phys.*, 2005, **7**, 3297–3305.

66 Y. Guo, K. Sivalingam, E. F. Valeev and F. Neese, SparseMaps—A systematic infrastructure for reduced-scaling electronic structure methods. III. Linear-scaling multireference domain-based pair natural orbital N-electron valence perturbation theory. *J. Chem. Phys.*, 2016, **144**, 094111.

67 Z. Chen, C. S. Wannere, C. Corminboeuf, R. Puchta and P. von R. Schleyer, Nucleus-Independent Chemical Shifts (NICS) as an Aromaticity Criterion. *Chem. Rev.*, 2005, **105**, 3842–3888.

68 J. O. C. Jiménez-Halla, E. Matito, J. Robles and M. Solà, Nucleus-independent chemical shift (NICS) profiles in a series

of monocyclic planar inorganic compounds. *J. Organomet. Chem.*, 2006, **691**, 4359–4366.

69 A. Stanger, Nucleus-Independent Chemical Shifts (NICS): Distance Dependence and Revised Criteria for Aromaticity and Antiaromaticity. *J. Org. Chem.*, 2006, **71**, 883–893.

70 A. C. Tsipis, Efficiency of the $NICS_{zz}$-scan curves to probe the antiaromaticity of organic and inorganic rings/cages. *Phys. Chem. Chem. Phys.*, 2009, **11**, 8244–8261.